Proc. 5th ASMO-UK/ISSMO Conf. on
Engineering Design Optimisation,
Stratford-upon-Avon, UK, 2004.

Shape optimization of the carotid artery bifurcation

Neil W. Bressloff[1], Alex I. J. Forrester[1], Jim Banks[1], K. Vijaya Bhaskar[1]
[1]*School of Engineering Sciences, University of Southampton,*
Highfield, Southampton, SO17 1BJ, UK.

email: N.W.Bressloff@soton.ac.uk

ABSTRACT

A parametric CAD model of the human carotid artery bifurcation is employed in an initial exploration of the response of shear stress to the variation of the angle of the internal carotid artery and the width of the sinus bulb. Design of experiment and response surface technologies are harnessed for the first time in such an application with the aim of developing a better understanding of the relationship between geometry (anatomy) and sites of arterial disease.

INTRODUCTION

The haemodynamic conditions that persist in the human carotid artery bifurcation are such that arterial disease commonly occurs in this region of the vascular system. Ultimately, the blockage that results from thickening of arterial walls (clinically referred to as stenosis) can rupture. The particles (emboli) that are produced can be carried in the bloodstream to the brain leading to stroke and fatality. Although there is much evidence for the correlation between sites of disease and the region of reversed flow in the internal carotid artery (ICA) [1], a greater understanding is needed of the impact different geometrical features of the bifurcation have on the likelihood and severity of disease. Such information will aid clinicians identify patients most at risk and also provide a basis for the design of grafts and stents.

The common carotid artery (CCA) bifurcates into two branches in the lower neck: the internal carotid artery (ICA) and the external carotid artery (ECA). Until relatively recently, many computer models of the carotid artery bifurcation (CAB) have treated it as Y-shaped and thus neglected the significance of straightening the flow relative to the CCA. Ding et al draw attention to the differences between the Y-shaped geometry and the so-called tuning fork model [2]. Interestingly, they claim that the Y-shaped geometry used by Bharadvaj et al [3] has become a standard in experimental and numerical investigations but they then proceed to show that a tuning-fork model represents a significant improvement particularly in relation to the correlation between the oscillatory shear index (OSI) and the location of intimal thickness. Thomas et al reinforce the preference for tuning-fork models especially for young healthy people [4]. The parametric CAD representations presented in this article are based upon a tuning-fork model of the bifurcation.

Numerous CFD simulations and in vitro analyses now provide much evidence for the correlations between locations of atherosclerosis and regions of low mean shear stress, high oscillation and high mean shear stress gradients [1, 5, 6]. Those studies that have investigated the impact of geometrical variations on flow features and on the correlations of these load metrics with sites of arterial disease are particularly relevant in the current context [7, 8].

Many other papers tend to use geometries derived from digitised images of real anatomy obtained from magnetic resonance imaging and ultrasound [9, 10]. Alternatively, bifurcation geometry is based on the experimental glass models described in [2] and [3]. Whereas previous work in this field has essentially provided information ascertained for discrete geometries, we aim to map complete landscapes relating shear stress metrics to CAB shape parameters. Here we focus on two parameters, the angle of the ICA and the width of the sinus bulb. Ultimately, we hope to apply the same techniques to many parameters simultaneously. The ICA angle is known to have a significant impact on the location and subsequent development of disease [7, 11, 12] and similar evidence is available for the shape of the bulb [13] and the area ratios of the ICA and ECA relative to the CCA [14].

The current work draws on techniques developed in aerodynamic design [15] to systematically investigate the relationship between the angle of the ICA and the width of the sinus bulb and a quantifiable measure of the region of reversed flow, the minimum time-averaged shear stress, $\bar{\tau}_{\min}$, where

$$\bar{\tau} = \frac{1}{T}\int \tau \, dt$$

and T denotes the period of a single pulse, τ signifies the instantaneous shear stress and t is time. An optimum geometry could be one in which $\bar{\tau}_{\min}$ is maximised, indicative of weaker recirculation.

OVERVIEW

A response surface modelling approach is adopted in which the design space is populated by an LP_τ design of experiments and the variation of $\bar{\tau}_{\min}$ is plotted using the method of kriging [16]. In order to systematically simulate the flow through a range of different bifurcations a software system is employed that automatically generates new geometries in CATIA V5 (Dassault System) from a baseline shape, constructs a suitable mesh in GAMBIT V2.1 (Fluent Inc.) and then solves the unsteady Navier-Stokes equations in FLUENT (Fluent Inc.).

Careful consideration of a number of geometry descriptions [2, 3, 17] shows that, from a CAD perspective, insufficient information is available in all of them to construct a parametric CAD model from scratch, without making a number of assumptions, and/or unrealistic constraints are imposed that limit the overall flexibility of the models. Consequently, we present a new parametric CAD definition of the tuning-fork geometry. There are some similarities with older models but a number of important innovations are introduced that yield a complete and reusable definition and provides sufficient flexibility to facilitate parametric (design) studies such as that described below. Thus, the baseline geometry is based on the tuning-fork glass models described in [2] but uses mean values tabulated in [3]. Hence, it effectively possesses a blend of the mean dimensions reported in [2] and [3]. The precise values are not critically important since the nature of the parametric model is such that any number of the defining parameters can be varied to yield an alternative geometry.

A mixture of splines and Bezier curves are used to control the bifurcation shape whereas a number of section definitions define the main bifurcation branches. Consequently, shape control through the bifurcation is achieved by adjusting the co-ordinates of the Bezier curve nodes. In this way, it is hoped that superior shape control can be achieved with a minimum number of parameters. A detailed description of the geometry definition is provided in the appendix.

The ICA angles vary between 9.80 and 41.0 degrees; this represents a range of three standard deviations symmetrically positioned either side of the mean. Bulb widths are less straightforward to define since the bulb shape is actually manipulated by the control points of Bezier curves. In this case, the parameter used to vary the bulb width is the x-coordinate of the control point of the outer ICA edge and its range of movement is set-up to produce an appropriate set of bulb shapes.

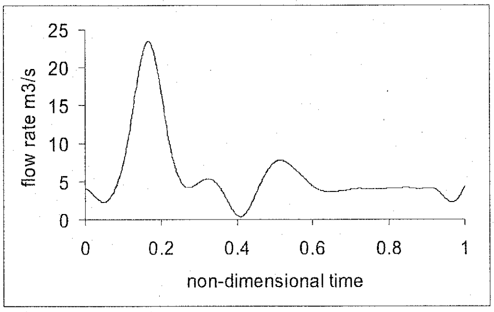

Figure 1: A typical pulse.

The mean pulse for the human carotid artery shown in Figure 1 is used [18] with a time-step of 0.0001s and the time-averaged shear stress, $\bar{\tau}$, is stored for each boundary surface. Meshes of between 25000 and 30000 cells are employed in each geometry. These spatial and temporal resolutions are consistent with those used in other sources and validated in mesh and time dependency studies performed prior to this article.

RESULTS AND DISCUSSION

Simulations for a 50 point LP_{τ} are performed using the relatively simple strategy depicted in Figure 2.

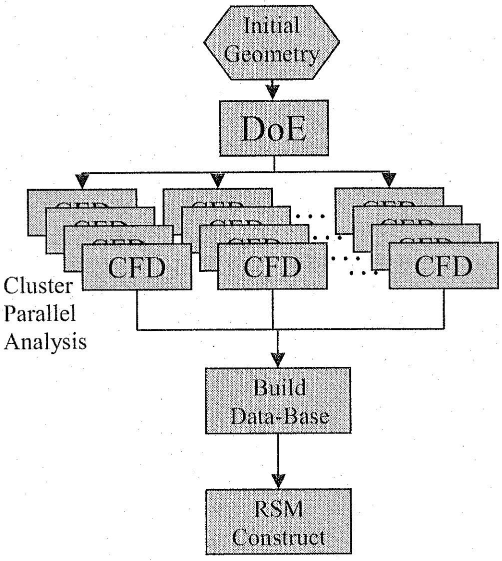

Figure 2: Response surface construction.

Figure 3 depicts snapshot streamlines for the geometry producing the lowest value of $\bar{\tau}_{\min}$. Similar flow patterns are present in all geometries with the strong systolic pulse initiating regions of recirculating flow that are then convected downstream.

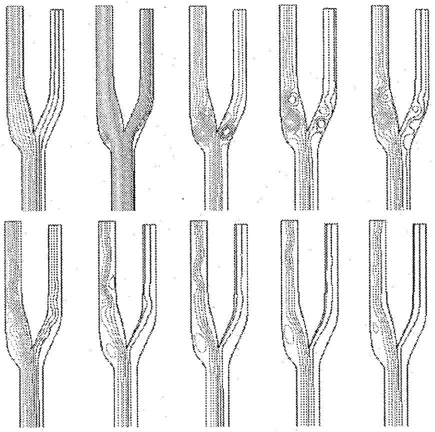

Figure 3: Typical streamline variation every tenth of a cycle.

Since, initially, we are more concerned to understand the complete landscape under examination than in determining the optimum, we construct response surfaces for 10, 20, 40 and 50 design points in Figures 4 to 7 to assess the convergence of the surface with number of desing points. Each surface has been constructed using the kriging method; the hyper-parameters have been tuned using a genetic algorithm followed by a dynamic hill climb.

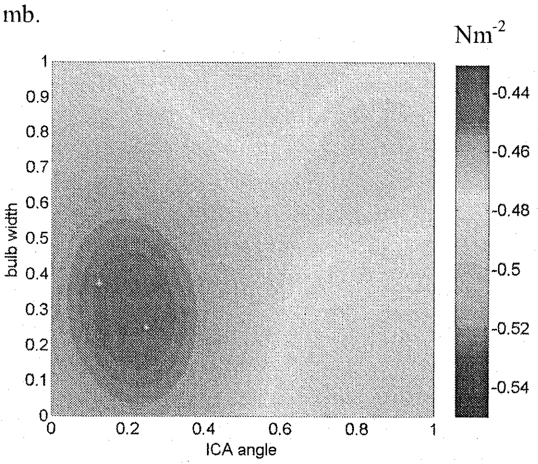

Figure 4: 10 point variation of $\bar{\tau}_{\min}$

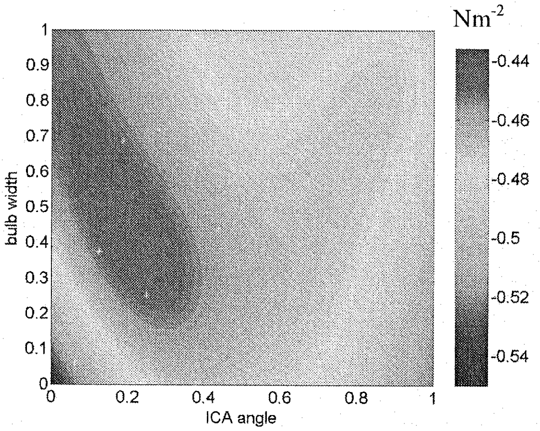

Figure 5: 20 point variation of $\bar{\tau}_{\min}$

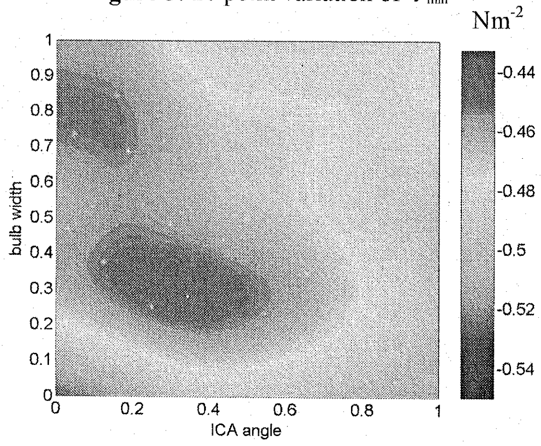

Figure 6: 40 point variation of $\bar{\tau}_{\min}$

Convergence of the response surface is clearly evident between successive numbers of design points both in terms of the approximate locations of high and low values of $\bar{\tau}_{\min}$. Surprisingly, $\bar{\tau}_{\min}$ appears to be minimised for small ICA angles and small bulb widths. Intuitively, one would expect a larger curvature change to produce stronger recirculation and, indeed, we find that larger angles and widths produce greater vorticity as evidenced in Figure 8.

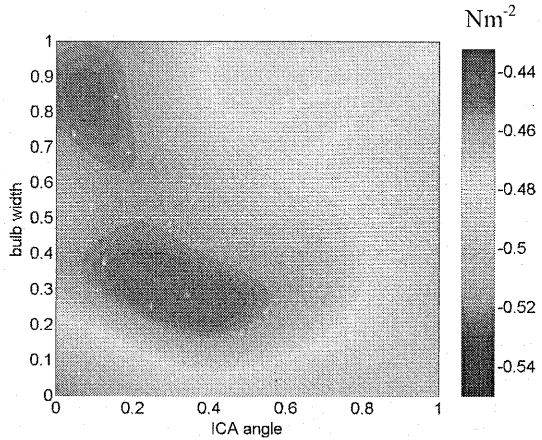

Figure 7: 50 point variation of $\bar{\tau}_{\min}$

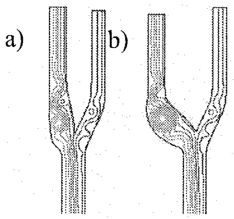

Figure 8: Streamlines of the flow at mid-points in the cycle for geometries with (a) small ICA angle and small bulb and (b) large ICA angle and large bulb.

However, the fact that we are exploring the spatial variation of a scalar (time-averaged) variable could be misleading. For example, although a larger curvature change may generate stronger vorticity, the nature of the high speed core flow (in the common carotid artery) of a geometry with more modest curvature variation, may concentrate its recirculating flow for longer in a particular position leading to lower $\bar{\tau}_{\min}$. Such an observation suggests that the choice of $\bar{\tau}_{\min}$ as an objective function may not be a good one. Figure 9 depicts the variation of time-averaged shear stress on the outer ICA wall for a range of bulb widths at a large ICA angle. Whereas there are relatively small differences in $\bar{\tau}_{\min}$ between geometries, there is a more significant variation in the area of negative mean shear stress, $\bar{\tau}_{-}$. Thus, alternative shear stress metrics are under investigation including spatially averaged integrals of $\bar{\tau}_{-}$ given by

$$\bar{\bar{\tau}} = \int \bar{\tau}\, dl_{-}$$

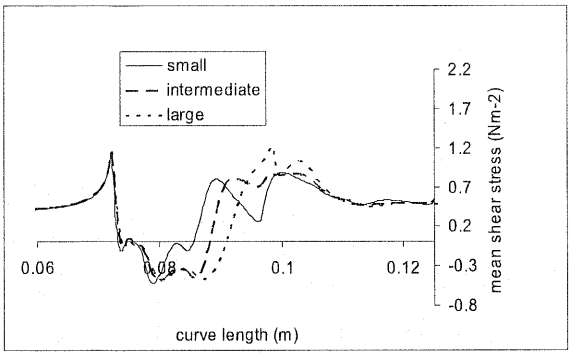

Figure 9: Variation of time-averaged shear stress on the outer ICA wall for a range of bulb widths at large ICA angle.

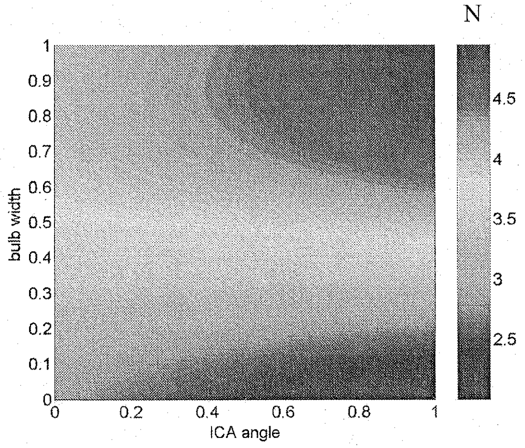

Figure 10: 9 point variation of $\bar{\bar{\tau}}$

Figure 10 shows a kriged response surface to the variation of $\bar{\bar{\tau}}$ though points at the corners of the domain, the mid-points of each outer edge and at the centre. Selection of boundary points in this way has proved useful in establishing the limits of exploration before committing to a full design of experiments (DoE). Although the surface requires refinement with updates and/or a full DoE, it is clear that the metric, $\bar{\bar{\tau}}$, produces more plausible results than the minimum value of the shear stress, $\bar{\tau}_{\min}$.

Consequently, on-going work is focussed on using $\bar{\bar{\tau}}$ and other similar metrics to explore the design space of the carotid artery bifurcation. We now have a three-dimensional parametric geometry definition for the tuning-fork model and are applying a search and update strategy as depicted in Figure A2 in the appendix. We are varying five parameters – the ICA and ECA angles, the bulb width and the ICA and ECA outflow diameters. Response surfaces are being constructed and tuned using kriging as described above and, parallel updates are being evaluated using maxiumum expected improvement [16].

CONCLUSIONS

The above analysis successfully applies response surface and design of experiment technologies to the exploration of the relationship between vascular anatomy and haemodynamics. Ultimately, it is hoped that such techniques will form the basis of an inverse design tool for identifying the likelihood and severity of disease for particular patients and, for the design of stents and grafts. However, results obtained so far for the variation of the minimum value of time-averaged shear stress, $\bar{\tau}_{\min}$, suggest that selection of suitable objective functions requires further work. Unexpectedly, $\bar{\tau}_{\min}$ is lowest for small ICA angles and bulb widths. A more plausible response is produced by the negative area of the mean shear stress curve.

REFERENCES

[1] Ku, D. N., Giddens, D. P., Zairns, C. K. and Glagov, S., 1985, Pulsatile flow and atherosclerosis in the human carotid bifurcation, Arteriosclerosis, 5, 3, 293-302.

[2] Ding, Z., Wang, K., Li, J. and Cong, X., 2001, Flow field and oscillatory shear stress in a tuning-fork-shaped model of the average human carotid bifurcation, J. Biomech. Eng., 34, 1555-1562.

[3] Bharadvaj, B. K., Mabon, R. F. and Giddens, D. P., 1982, Steady flow in a model of the human coarotid bifurcation. Part I – Flow visualisation, J. Biomechanics, 15, 5, 349-362.

[4] Thomas, J. B., Che, S. L., Milner, J. S., Antiga, L., Rutt, B. K., Spence, J. D. and Steinman, D. A., 2003, Summer Bioengineering Conf., Florida, USA.

[5] Buchanan, J. R. Jr. and Kleinstreuer, C., 1998, Simulation of particle-hemodynamics in a partially occluded artery segment with implications to the initiation of microemboli and secondary stenoses, J. Biomech. Eng., Trans. ASME, 120, pp. 446-454.

[6] Zairns, C. K., Giddens, D. P., Bharadvaj, B. K., Sottiurai, V. S., Mabon, R. F. and Glagov, S., 1983, Carotid bifurcation atherosclerosis, Circ. Res., 53, 4, 502-514.

[7] Perktold, K., Peter, R. O., Resch, M. and Langs, G., 1991, Pulsatile non_Newtonian blood flow in three-dimensional carotid bifurcation models: a numerical study of flow phenomena under different bifurcation angles, J. Biomed. Eng., 13, 507-515.

[8] Wells, D. S., Archie, J. P. and Kleinstreuer, C., Effect of carotid artery geometry on the magnitude and distribution of wall shear stress gradients, J. Vasc. Surg., 667-678, 1996.

[9] Milner, J. S., Moore, J. A., Rutt, B. K. and Steinman, D. A., 1998, Hemodynamics of human carotid artery bifurcations: Computational studies with models constructed from magnetic resonance imaging of normal subjects, J. Vasc. Surg., 28, 1, 143-156.

[10] Augst, A. D., Barratt, D. C., Hughes, A. D., Thom, S. A. M. and Xu, X. Y., 2003, Various issues relating to computational fluid dynamics simulations of carotid bifurcation flow based on models reconstructed from

three-dimensional ultrasound images, Proc. Inst. Mech. Eng. Part H – J. Eng. Med., 271, 5, 393-403.

[11] DeSyo, D., 1989, Radiogrammetric analysis of carotid bifurcation: Hemodynamic-atherogenetic repercussions on surgical practice, Proc. 2nd Int. Sump. Biofluid Mech. Biorheology, Munich, 71-72.

[12] Sitzer, M., Puac, D., Buehler, A., Steckler, D. A., von Kegler, S., Markus, H. S. and Steinmetz, H., 2003, Internal carotid artery angle of origin – A novel risk factor for early carotid atherosclerosis, Stroke, 34, 4, 950-955.

[13] Perktold, K and Resch, M., 1990, Numerical flow studies in human carotid artery bifurcations: basic discussion of the geometric factors in atherogenesis, J. Biomed. Eng., 12, 111-123.

[14] Fisher, M. and Fieman, S., 2000, Geometric factors of the bifurcation in carotid atherogenesis. Stroke, 21, 267-271.

[15] Forrester, A. I. J., Bressloff, N. W. and Keane, A. J., 2003, Response surface model evolution, 16th AIAA Computational Fluid Dynamics Conference, AIAA-2003-4089, Orlanda, USA.

[16] Jones, D. R., 2001, A taxonomy of global optimization methods based on response surfaces, *J. Glob. Opt.*, 21, 345-383.

[17] Fanucci, E., Orlacchio, A. and Pocek, M., 1988, The vascular geometry of human arterial bifurcations, Inv. Radiology, 23, 10, 713-718.

[18] Holdsworth, D. W., Norley, C. J. D., Frayne, R., Steinman, D. A. and Rutt, B. K., 1999, Characterization of common carotid artery blood-flow waveforms in normal human subjects, Physiol. Meas., 20, 219-240.

APPENDIX

Tuning fork geometry definition

The parametric CAD definition uses the junction between the inner walls of the ICA and ECA as the origin and starting point of the construction. Figure A1 depicts the complete definition. First, lines OA and OB are drawn from the origin, O, for the ECA and ICA, respectively, that define the orientations and the respective widths at the bifurcation. The CCA is also defined relative to O with an offset for its centre-line. It can be seen that the ICA and ECA both return to paths that are parallel with the CCA.

The co-ordinates of the Bezier control points and the co-ordinates of other defining points of the ICA and ECA are tabulated for the baseline geometry in Table 1 and the values of the various parameters are listed in Table 2. Starting with the ICA, the following comments accompany these definitions.

1) ICA Bezier curve end-points. The end-point, C, of the inner curve in Figure A1 is based on a blend between the ways in which the distance OC is defined in the Bharadvaj et. al. and Ding et. al. papers. Relative to C, the outer curve end-point, D, is positioned a distance, CD away in order to accommodate an interface region between the bulb and the straight outflow of width GH. CD > GH so that the shape of the Bezier curves are not over constrained.

2) Bezier curve control points. Two control points are used for each of the ICA Bezier curves. For the outer curve, the distance of Po1 above point B is specified by the height of a right-angle triangle drawn with its hypotenuse on BD and of a parametric length, dmax bulge, equivalent to the position of the maximum bulb width in Bharadvaj et. al. The y-coordinate of the control point Pi1 for the inner ICA curve is evaluated in the same way but along the line OC. The x-coordinates of Po1 and Pi1 are then set relative to B and O, respectively, using parameters d_{outer} and d_{inner}. The second control points for each curve are required to control the tangency constraint in to the interface region. Suitable positions for Po2 and Pi2 are a fixed distance below points D and C, respectively.

3) ICA interface. A suitable interface region between the bulb and the straight section of the ICA tapers from a width, CD to the outflow width, EF over a length d_{int}.

4) ICA straight section. The straight section, of length d_{str}, is such that EF = GH.

5) ECA curvature. Splines are used to define the shape of the curved ECA section. Relative to points O and A, the other end-points, I and J, are constructed in the same way as points C and D for the ICA. Intermediate points, K and L, are fixed a distance, d_{ccurve}, along lines drawn from O and A, respectively, and parallel to the direction of the ECA.

6) ECA interface and straight section. These are defined in the same way as for the ICA with IJ > MN = PQ and with the same lengths, d_{int} and d_{str}.

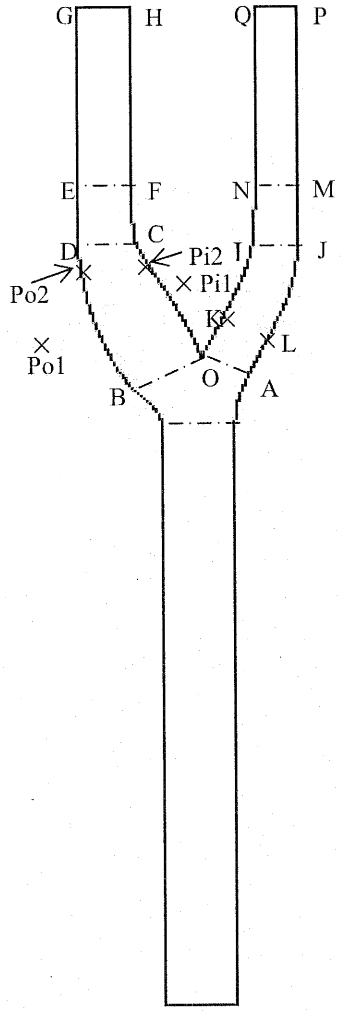

Figure A1 Tuning fork geometry definition.

Point	x co-ordinate	y co-ordinate
B	$B_x = O_x - w_{OB}\cos(\theta_i)$	$B_y = O_y - w_{OB}\sin(\theta_i)$
C	$C_x = O_x - \frac{180g}{\pi\theta_i}\frac{\sin^2(\theta_i)}{\sin(90-\theta_i/2)}$	$C_y = O_y + \frac{180g}{\pi\theta_i}\frac{\sin(\theta_i)\cos(\theta_i)}{\sin(90-\theta_i/2)}$
D	$D_x = C_x - w_{CD}$	$D_y = C_y$
E	$E_x = D_x$	$E_y = D_y + 1$
F	$F_x = E_x + w_{EF}$	$F_y = E_y$
G	$G_x = E_x$	$G_y = E_y + d_{str}$
H	$H_x = F_x$	$H_y = G_y$
P_{o1}	$P_{o1x} = B_x - d_{\max bulge}\sin(\theta_i) - d_{outer}$	$P_{o1y} = B_y + d_{\max bulge}\cos(\theta_i)$
P_{i1}	$P_{i1x} = O_x - d_{\max bulge}\sin(\theta_i) - d_{inner}$	$P_{i1y} = O_y + d_{\max bulge}\cos(\theta_i)$
P_{o2}	$P_{o2x} = D_x$	$P_{o2y} = D_y - 4/15$
P_{i2}	$P_{i2x} = C_x$	$P_{i2y} = C_y - 4/15$
A	$A_x = O_x + w_{OA}\cos(\theta_e)$	$A_y = O_y - w_{OA}\sin(\theta_e)$
I	$I_x = O_x + \frac{180g}{\pi\theta_i}\frac{\sin(\theta_i)\sin(\theta_e)}{\sin(90-\theta_i/2)} - \frac{3}{16}$	$I_y = O_y + \frac{180g}{\pi\theta_i}\frac{\sin(\theta_i)\cos(\theta_e)}{\sin(90-\theta_i/2)}$
J	$J_x = I_x + w_{IJ}$	$J_y = I_y$
K	$K_x = O_x + d_{ecurve}\sin(\theta_e)$	$K_y = O_y + d_{ecurve}\cos(\theta_e)$
L	$L_x = A_x + d_{ecurve}\sin(\theta_e)$	$L_y = A_y + d_{ecurve}\cos(\theta_e)$
M	$M_x = J_x$	$M_y = J_y + 1$
N	$N_x = M_x - w_{MN}$	$N_y = M_y$
P	$P_x = M_x$	$P_y = M_y + d_{str}$
Q	$Q_x = N_x$	$Q_y = P_y$

Table 1. Co-ordinate definitions for the tuning-fork model (cf. Figure A1).

Parameter	Default value
θ_i	25.4 degrees
θ_e	25.1 degrees
w_{c0}	8.00mm
w_{OB}	1.04
$d_{max\ bulge}$	0.91
d_{int}	2.14
d_{outer}	-0.0019
d_{inner}	0.0011
w_{CD}	0.75
w_{EF}	0.7125
d_{str}	2.5
w_{OA}	0.69
d_{ecurve}	0.91
w_{IJ}	0.6053
w_{MN}	0.575

Table 2. Default parameters for baseline tuning-fork model. All widths, *w*, and lengths, *d*, are non-dimensionalised by the CCA width, w_{c0}. The subscripts refer to locations shown in Figure A1 with appropriate definitions provided in the text.

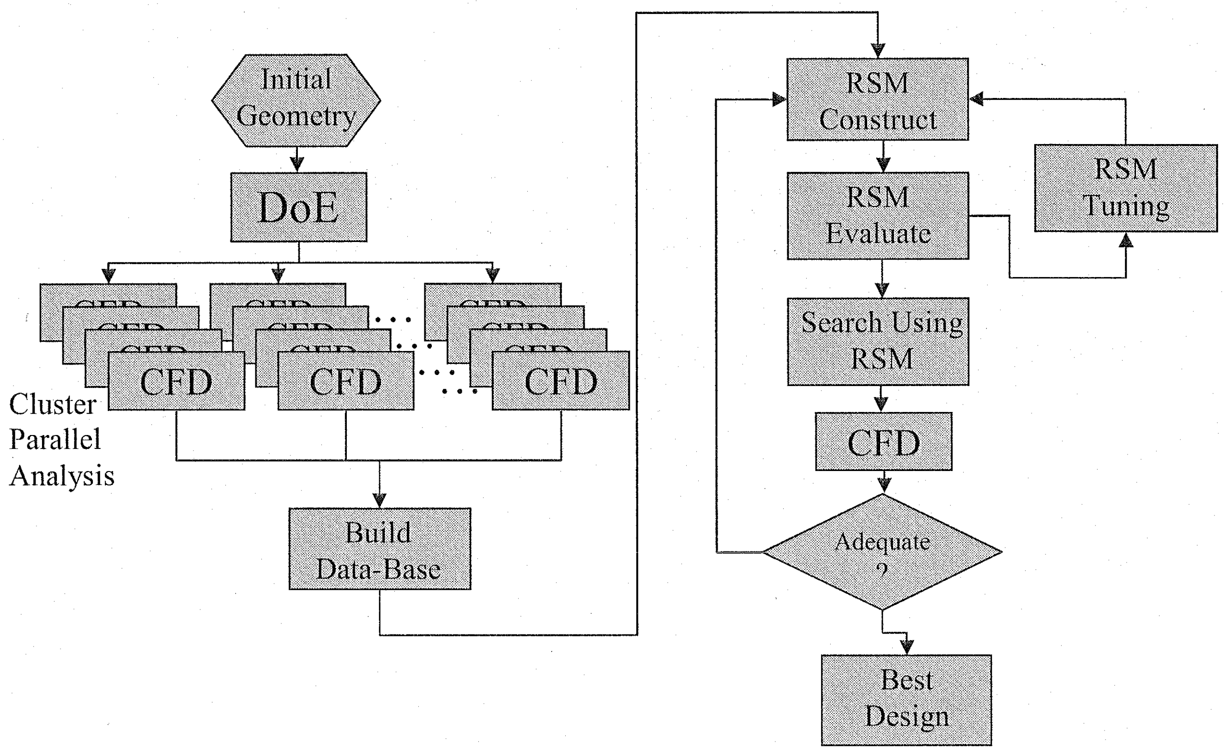

Figure A2 Parallel update strategy.